ELSEVIER

Journal of Fluids and Structures 25 (2009) 1258–1271

JOURNAL OF FLUIDS AND STRUCTURES

www.elsevier.com/locate/jfs

Interaction of a line vortex with a round parachute canopy

H. Johari[a,*], A. Levshin[b]

[a]Department of Mechanical Engineering, California State University, Northridge, CA 91330, USA
[b]Department of Mechanical Engineering, Worcester Polytechnic Institute, Worcester, MA 01609, USA

Received 17 August 2008; accepted 24 July 2009
Available online 11 September 2009

Abstract

The interaction of a rectilinear vortex with an inflated round parachute canopy model was studied experimentally in a water tunnel where the vortex core was aligned with the axis of the canopy. Three different canopy diameters were used, and the canopy model was attached to a streamlined forebody. Dye flow visualization indicated that vortex breakdown was present when the core trajectory was within the canopy opening. Vortex breakdown occurred about one to two canopy diameters upstream of the canopy opening. The vortex core completely disintegrated when it interacted with the forebody near the canopy centerline. The vortex breakdown and disintegration caused unsteady, asymmetric deformations on the canopy surface. A reduction in the time-averaged drag and an increase in the fluctuating drag was observed when the vortex core was within the canopy opening. The disintegration of the vortex core near the canopy centerline lessened the drag reduction brought on by the presence of the core.

Keywords: Vortex interaction; Parachute canopy dynamics; Deformable bluff body drag

1. Introduction

Round solid cloth parachute canopies used for personnel and cargo routinely come in contact with vortices in their surroundings. These vortices, which are generated upstream of the canopy, may have a significant effect on the primary function of the parachute. Under certain conditions, such interactions can lead to the complete collapse of the canopy. The use of multiple aircraft in tight formation is also required for specific operations. In such cases, the parachute canopy of a paratrooper may encounter and interact with vortices in the aircraft wake and/or those generated by the parachute canopy of others below him. The interaction may result in partial or complete collapse of the parachute canopy.

Primary sources of upstream vortices that can significantly affect the operation of an inflated parachute canopy are: the control surfaces on the aircraft carrying the parachute, the wing tip vortices of the leading aircraft during multi-ship airdrops, and the vortices shed in the wake of a canopy located upstream of the one under consideration. The latter scenario is particularly troublesome when a large number of parachutes are closely spaced. As the canopy inflation typically initiates in a horizontal orientation and the canopy subsequently rotates to a vertical orientation, it is possible that a parachute canopy may encounter vortices in various orientations. Vortices may interact with parachute canopies in one of the two canonical categories: parallel or perpendicular. In the former, the vortex core is parallel to the canopy

*Corresponding author. Tel.: +1 818 677 3099; fax: +1 818 677 7062.
E-mail address: hjohari@csun.edu (H. Johari).

0889-9746/$ - see front matter © 2009 Elsevier Ltd. All rights reserved.
doi:10.1016/j.jfluidstructs.2009.07.005

axis, whereas in the latter, the vortex core is perpendicular to the canopy axis. These two idealized cases are depicted schematically in Fig. 1

A literature search indicated that significant progress has been made in the area of vortices interacting with solid surfaces such as fins (Wolfe et al., 1995; Lambert and Gursul, 2004), streamlined (Bodstein et al., 1996) and bluff bodies (Sun and Marshall, 2000). The subject of vortex interactions has been reviewed by Rockwell (1998), and a majority of studies in this area are in the context of helicopter blade–vortex interactions. Even though there is recent interest in flexible structures such as flapping foils (Heathcote et al., 2008), little is known about the interaction of a vortex with a deformable body such as an inflated parachute canopy. Vortex interactions in such cases can lead to a substantial modification of the body, whereas in the rigid body case the geometry of the body remains intact. Computational approaches for deformable bodies employ the currently available large computational resources and coupled algorithms which have been advanced recently (Gluck et al., 2003; Longatte et al., 2009).

The various features associated with parachute canopies going from inflation to terminal descent have been reviewed by Strickland and Higuchi (1996) and Peterson et al. (1996). One of the interesting features of the canopy dynamics during terminal descent is the 'breathing' where the canopy diameter fluctuates about a mean value. This is caused by the interaction of the vortices shed from the canopy with the flexible fabric (Johari and Desabrais, 2005). Experimental studies concerned with the interaction of swirling flow fields with parachute canopies include those by Blake (1996) and Rogers and Kididis (1997). The latter study exposed scaled model parachutes to the swirling flow of a fan. The experiments were carried out in a vertical wind tunnel, and the canopy symmetry axis was perpendicular to the fan flow direction. The experiment indicated that in the perpendicular vortex-canopy category, the velocity gradient may be more important than the magnitude of the cross-flow. The model canopy collapsed completely when the fan velocity was in the range of 1.3–2 times the canopy descent velocity. However, to our knowledge, there has not been any previous studies of the interaction of an inflated round parachute canopy with a well-defined, rectilinear vortex that is aligned with the canopy axis. Thus, an experimental investigation of such an interaction was pursued.

The primary objective of the present study was to examine the interaction of a distinct, streamwise rectilinear vortex aligned with an inflated, solid cloth round parachute canopy. The experiments are intended to simulate the parallel interaction scenario in a controlled laboratory environment, and to investigate the resulting impact on the canopy geometry and drag. The experiments were carried out in a low-speed water tunnel where the canopy diameter, canopy–vortex separation, and freestream velocity were systematically varied. The vortex was formed by a half-wing placed in the tunnel. The canopy was placed in the near field of the tip vortex where the circulation and core size remained nearly constant.

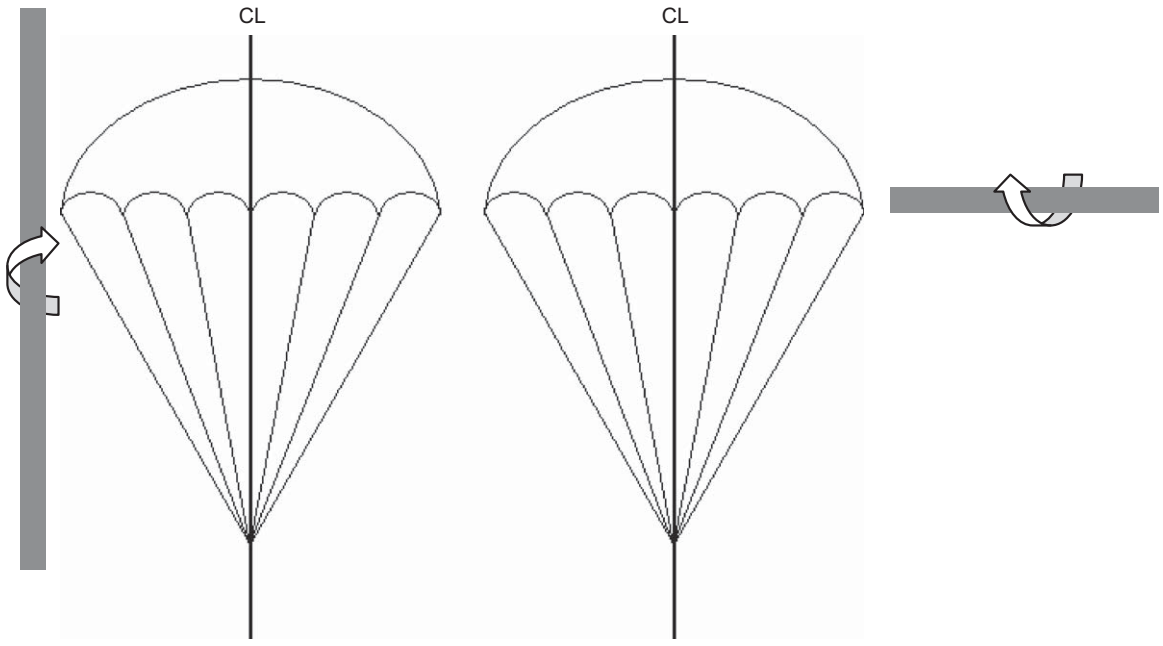

Fig. 1. Idealized canopy–vortex interaction: parallel (left) and perpendicular (right).

2. Dimensionless parameters

The interaction of an inflated canopy with a line vortex is characterized by dimensionless parameters formed by the vortex strength and position as well as the canopy specifics. The key parameters of a line vortex are its circulation, Γ, and core radius, σ. Other relevant parameters are the distance between the vortex core and the canopy symmetry axis, s, as well as the angle between the vortex and the canopy axis. This angle was nominally zero in the present experiments as the vortex was aligned with the streamwise direction and parallel to the canopy axis. The axial velocity, w, in the vortex core is another parameter associated with line vortices.

The parameters expressly associated with the canopy are the mean projected diameter of the inflated canopy, D_p, pressure differential across the fabric, fabric permeability, canopy Reynolds number, as well as canopy mass and stiffness. The mean projected diameter of circular, solid cloth canopies is typically 0.67–0.7 times the constructed (flat) diameter, D_o (Knacke, 1992). The small-scale models used in the experiments have similar projected diameter ratios. The pressure differential across the canopy fabric scales with the freestream dynamic pressure because the flow inside the canopy is nearly stagnant, and there is a small amount of suction on the exterior surface due to the passage of vortical structures. Fabric permeability is typically characterized by the average velocity across the fabric for a prescribed pressure differential (typically $\frac{1}{2}$ in of water in the US). For full-scale parachutes, the mean flow velocity through the fabric is a small fraction (few percent) of the freestream velocity. The permeability is likely to have a minor effect on the canopy–vortex interaction. Furthermore, findings from earlier experiments with similarly sized models have indicated that small-scale impermeable fabric canopies behave quite close to those made with the standard low permeability fabric (Desabrais and Johari, 1999).

The Reynolds number, based on the canopy constructed diameter, D_o, and the freestream velocity, U, ranged from 45×10^3 to 91×10^3 in the interaction experiments. For the canopy Reynolds numbers considered here, the flow separates from the lip of a fully inflated canopy and increasing the Reynolds number does not alter the separation location. However, there might be secondary effects associated with the canopy Reynolds number.

In fluid–structure interaction problems, the ratio of structure to fluid density is an important parameter. In parachute literature, the mass ratio parameter, $m/\rho {D_o}^3$, is used instead. In this expression, m is the canopy mass and ρ the fluid density. Large scale canopies in air have mass ratios of $\sim10^{-3}$ and smaller, whereas the model canopies in the present experiments have mass ratios of $1\text{–}2\times10^{-4}$. Although the mass ratios in the experiments are about an order of magnitude smaller than those of large scale canopies in air, all these values are significantly less than one. The very small values of mass ratio imply that the inertia of the canopy fabric does not play a major role in the problem.

The canopy stiffness can be quantified through the index η developed by Heinrich and Hektner (1971). The stiffness index is defined as $\eta=(D_{\max}/D_o)(m/\rho_a S_o)$, where $D_{\max}$ is the maximum canopy width when hung upside down, S_o is the canopy surface area, and ρ_a is the fabric areal density. The stiffness index was equal to $D_{\max}/D_o$ as a result of the simple construction used in making the model canopies in the present experiments. The model canopies were hung upside down and $D_{\max}$ was measured visually. As noted in the next section, the small-scale canopies used in the experiments had indices which were approximately three times that of full-scale canopies. However, canopy performance has been shown to be a weak function of the canopy stiffness especially during steady descent (Johari and Desabrais, 2003).

The following important dimensionless parameters emerge from the above discussions: (i) separation distance, s/D_p, (ii) vortex core size to canopy diameter ratio, σ/D_p, (iii) Reynolds number, $\mathrm{Re}=UD_o/\nu$, and (iv) relative vortex strength, $\Gamma/2\pi\sigma U$. The last parameter is derived from the pressure deficit in the core of a Rankine vortex ($\rho\Gamma^2/4\pi\sigma^2$) normalized by the pressure differential across the canopy fabric, which scales with ρU^2. Dividing the last two parameters and taking the square root results in $\Gamma/2\sqrt{\pi}\sigma U$; however, for simplicity the square root of π was replaced by π. The relative vortex strength parameter $\Gamma/2\pi\sigma U$ is significant, given that deformation of the canopy is a result of the modification of the surface pressure differential distribution. It is expected that significant deformations of the inflated canopy would appear when this parameter is of the order of 1. Estimates of σ/D_p for practical parachutes result in values on the order of 0.02–0.2.

In the present experiments, the parameter s/D_p was varied by the changes in the separation distance. The differences in the diameters of three model canopies provided for σ/D_p and Re variations. The normalized vortex strength $\Gamma/2\pi\sigma U$ was constant at each freestream velocity by fixing the angle of attack of the half-wing creating the line vortex.

3. Experimental technique

3.1. Set-up

The experiments were conducted in a low-speed water tunnel with a square test-section of $0.6\times0.6\,\mathrm{m}^2$ cross-section and a 2.4 m length. The tunnel freestream velocity was varied between 0.10–0.30 m/s. The freestream turbulence

intensity was less than 1.3% over this operating range. Optical access was available through the transparent test-section walls.

Three flat circular canopies with diameters $D_o = 6$ in (152 mm), 9 in (229 mm), and 12 in (305 mm) were constructed from a single piece (instead of individual gores) of standard (1.1 oz/yd^2) rip-stop nylon fabric. 100-μm nylon thread suspension lines were attached to the edge of the model canopies. The length of suspensions lines was equal to the constructed diameter of the canopy models. The projected diameter of these models ranged from 107 to 214 mm. Models fabricated in this manner had relatively low stiffness indexes, as defined by Heinrich and Hektner (1971), of $\eta = 0.5$ and 0.43 for the 6- and 12-in models, respectively. The difference in the stiffness index of the three models is fairly small (<15%). In comparison, a 28-foot parachute canopy has an index of 0.15.

An inflated canopy and the supporting hardware in the water tunnel are shown in Fig. 2. The model canopies were positioned horizontally in the water tunnel. The canopy was attached by 24 suspension lines to a streamlined forebody which had a diameter of 0.5 in (12.7 mm) and a length of approximately 4.2 in (107 mm). The forebody cross-sectional area was less than 1.5% of the 6-in canopy projected area. The streamlined forebody minimized the effects of its wake. The forebody was attached to a 3/8 in (9.5 mm) stainless steel shaft which transferred the loads to a 6-component load cell outside the water tunnel. To reduce the effects of the drag contributed by the shaft and the associated vortex shedding, a $\frac{3}{4}$ in (19 mm) thick streamlined sheath of 1.65 in (42 mm) length was used. Vortex shedding was not observed in the sheath wake.

Flat circular canopy geometries are known to have off-axis oscillations during terminal descent. In order to eliminate the off-axis oscillations, a 0.5 mm diameter flexible nylon retention line was attached to the sheath and passed through the apex of the canopy. The end of the retention line was held rigidly far downstream of the canopy. The retention line restrained the canopy wandering, without adversely affecting the flexible nature of the canopy.

3.2. Drag measurement

Drag on the canopy and forebody was measured by the load cell, and the loads due to the supporting hardware and the forebody were extracted from the data. Drag on the canopy and suspension lines was denoted by F. The load cell output was sampled with a 16-bit A/D card, and 20 000 data points were collected for each experimental condition. The uncertainty of the measured data was 0.01 N. The time-averaged drag coefficient of the canopy was defined by

$$C_D = \frac{\bar{F}}{q_o(\pi/4)D_o^2}, \tag{1}$$

using the canopy constructed area ($\pi {D_o}^2/4$), the dynamic pressure $q_o = \frac{1}{2}\rho U^2$, and the time averaged force $\bar{F}$. To assess the fluctuating component of drag, the root-mean-square (rms) of the F fluctuations was normalized as follows:

$$C'_{D\ \mathrm{rms}} = \frac{F'_{\mathrm{rms}}}{q_o(\pi/4)D_o^2}. \tag{2}$$

The time averaged and fluctuating drag of the canopy are presented in the Results section.

The uncertainty of load cell data translates to drag coefficient uncertainties ranging from 3.5% for the 6-in model at 0.2 m/s to 0.3% for the 12-in model at 0.3 m/s. On the other hand, the data for the 6-in model at 0.1 m/s had large uncertainties (18%), and were not considered. The uncertainty was less than 5% for all the data presented here.

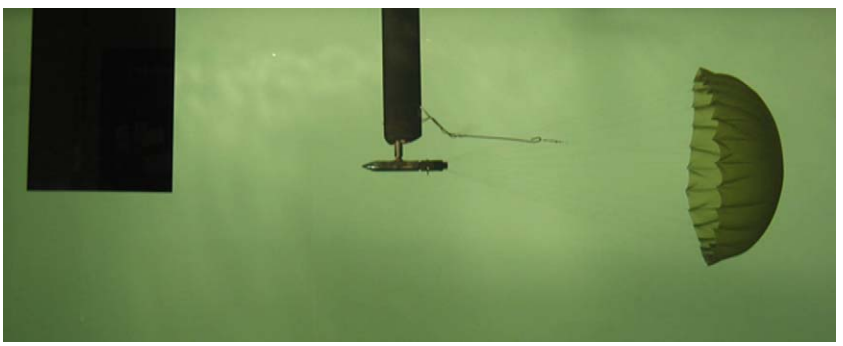

Fig. 2. The 12-in canopy in the water tunnel with the forebody and support structure. The wing tip is visible upstream of the model canopy.

Standard methods for calculation of the blockage ratio for bluff bodies and parachute canopies in closed wind/water tunnels employ the projected area of the canopy divided by the tunnel cross-sectional area (Maskell, 1965; Cockrell, 1987). Based on the mean projected diameter of the canopy models in the experiments, blockage ratios were 2.5%, 5.6%, and 9.9% for the 6-, 9-, and 12-in models, respectively. Cockrell (1987) states that blockage ratios up to 10% can be readily corrected using Maskell's method. Macha and Buffington (1989) provide the following expression for the tunnel dynamic pressure correction, based on Maskell's method. The dynamic pressure, was corrected by

$$q_o = q_{o_u}\left[1 + K_M \frac{C_{D_u} S_p}{S_T}\right], \tag{3}$$

where q_{o_u} is the uncorrected dynamic pressure, K_M is an empirically derived blockage factor (= 1.85 for flat circular canopies), C_{D_u} is the uncorrected drag coefficient of the canopy, S_p is the projected area of the canopy diameter, and S_T is the test-section cross-sectional area.

3.3. Line vortex

The tip vortex generated by a half-wing with a chord length of $c = 6$ in (152 mm) and a NACA 6409 profile was used as the line vortex in the experiments. This profile, as opposed to other classical profiles, was chosen because it created a strong tip vortex for the present experimental conditions. A fixture which allowed precise positioning of the wing tip with respect to the canopy/forebody centerline held the half-wing in the tunnel. The half-wing had a wetted span of 12 in, resulting in an effective aspect ratio of 4. A side view of the half-wing in the water tunnel, upstream of the 12-in canopy model, is visible in Fig. 2 Throughout the experiments, the half-wing angle of attack was fixed at 12°. This angle of attack had the largest lift coefficient prior to stall for the Reynolds numbers considered here (Selig et al., 1989). The canopy lip was approximately $3.5c$ away from the trailing edge of the wing. The flow in the vortex core and near the vicinity of the canopy was visualized by water soluble dye. The tip vortex was fully formed at this location, and negligible wandering was observed in the absence of the canopy.

The vortex flow field was quantified by the Particle Image Velocimetry (PIV) technique in a plane perpendicular to the freestream flow to enable the calculation of the streamwise vorticity. The time-averaged vorticity field is shown in Fig. 3 at a freestream velocity of $U = 0.3$ m/s. Clearly the vorticity is concentrated in the vortex core even though vorticity is also present in the wake of the half-wing, as depicted by the vertical strip on the right-hand side. From the data, the peak vorticity was determined to be $\omega_o = 31\,\mathrm{s}^{-1}$ and the circulation was $\Gamma = 0.025\,\mathrm{m}^2/\mathrm{s}$. The vorticity field was not symmetric, particularly away from the core; however, the distribution within the central portion of the vortex was close to a Gaussian. Assuming a Gaussian distribution of vorticity in the vortex core, the following expression was used to compute the vortex radius:

$$\sigma = \sqrt{\Gamma/\pi\omega_o}. \tag{4}$$

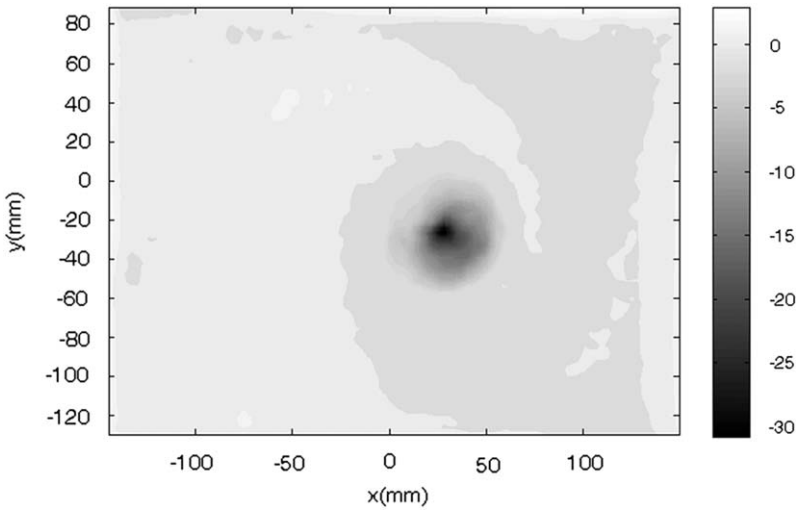

Fig. 3. Streamwise vorticity field of the tip vortex. The scale is in s^{-1}.

The computed radius for the vortex in Fig. 3 was $\sigma = 16\,\text{mm}$. This computed vortex core size can be compared with the value of 11 mm observed visually from the dye streaklines. Using the measured values of vortex circulation $\Gamma = 0.025\,\text{m}^2/\text{s}$ and radius $\sigma = 16\,\text{mm}$, the parameter $\Gamma/2\pi\sigma U$ was computed to be $0.83(\pm 9\%$ uncertainty) for the conditions in Fig. 3, namely $U = 0.3\,\text{m/s}$. For the other freestream velocity of $U = 0.2\,\text{m/s}$, the relative vortex strength was $\Gamma/2\pi\sigma U = 0.69 \pm 12\%$. Even though the vortex circulation varies linearly with the freestream velocity U, the radius of the vortex depends on the velocity. Based on the computed vortex radius, the parameter σ/D_p ranged from 0.15 to 0.075 at $U = 0.3\,\text{m/s}$ and from 0.18 to 0.09 at the $U = 0.2\,\text{m/s}$ freestream velocity for the 6- and 12-in canopy models, respectively.

4. Results

4.1. Visualization

The interaction of the vortex with the 12-in canopy at a Reynolds number of 9.1×10^4 and at three different spatial separations is presented in Fig. 4 The vortex was visualized by dye released at the wing tip. In Fig. 4(a) the vortex core was at $s/D_p \approx 0.7$ upstream of the canopy, i.e. outside the canopy opening. As the vortex approached the canopy, the core was deflected due to the curvature of the streamlines around the canopy. The core remained coherent and was nearly unaffected as it moved around the canopy, as evident in Fig. 4(a). The same was observed for all three canopies while $s/D_p > 0.5$. When the vortex trajectory fell within the canopy projected area, the vortex broke down in the classical sense where the core diameter expanded and turbulent motion was present inside the core (Leibovich, 1978). Vortex breakdown occurred approximately 1–2 canopy diameters upstream of the canopy. This was due to the deceleration caused by the canopy presence. Vortex breakdown, which was observed for all three canopy models, resulted in the rapid enlargement and undulation of the vortex core. In Fig. 4(b), the vortex core was nominally at $s/D_p \approx 0.45$ as it approached the canopy lip. The difference in the visualized vortex core diameter in Figs. 4(a) and (b) is considerable.

As the enlarged, turbulent vortex core moved toward the center of the canopy and the vicinity of the forebody, the vortex core disintegrated and produced large parcels of vortical flow covering nearly the entire streamtube approaching the canopy opening. The image in Fig. 4(c) corresponds to $s/D_p \approx 0.06$; vortex breakdown occurred upstream of the forebody. Subsequently, the core disintegrated into large-scale unsteady vortical parcels which interacted with the canopy. The lines drawn on the image in Fig. 4(c) indicate the approximate extent of the dyed vortical flow reaching the canopy. Large deformations of the canopy were observed when the vortex core interacted with the forebody. Vortex breakdown caused lateral motions of the canopy for the smallest canopy (6-in) model even though the apex was rigidly held.

Response of the canopy to the presence of the line vortex is shown in Fig. 5. The 12-in canopy was quite symmetric in Fig. 5(a) in absence of the vortex at a Reynolds number of 9.1×10^4. All three canopies experienced 'breathing', a nearly periodic expansion and contraction of the canopy diameter. Negligible changes in the canopy geometry were observed while the vortex core was outside the canopy opening, $s/D_p > 0.5$. When the core was placed at the canopy lip or inside the canopy ($s/D_p \leq 0.5$), deformations of the canopy became apparent. The loss of symmetry can be observed in the two instantaneous images of Fig. 5(b). The appearance of asymmetry on top of the canopy at different locations is noteworthy. The undulating vortex core, which underwent breakdown upstream of the canopy, appeared to have excited non-axisymmetric modes of the canopy. The geometry of the canopy deformation varied with time even though the core was stationary upstream of the canopy.

Appreciable deformations of the canopy are visible in Fig. 5(c) with the vortex core near the centerline and interacting with the forebody and the canopy. As noted earlier, in this case the vortex core disintegrated into large scale vortical parcels spread over the entire canopy opening. Although the vortex position upstream of the canopy was the same for the two instantaneous images in Fig. 5(c), the considerable bulge moved around the canopy surface. The dynamics of the canopy surface deformations was qualitatively the same for all cases when the vortex core was within the canopy opening. The effects of the canopy–vortex interaction on the canopy drag are discussed in the following sections.

4.2. Baseline drag

The drag on the model canopies in absence of the vortex was measured to assess the baseline characteristics of the three canopies. The time averaged drag as a function of the canopy Reynolds number is presented in Fig. 6 The data indicate an increasing trend for C_D with Reynolds number. For Reynolds numbers greater than 4.5×10^4, the drag

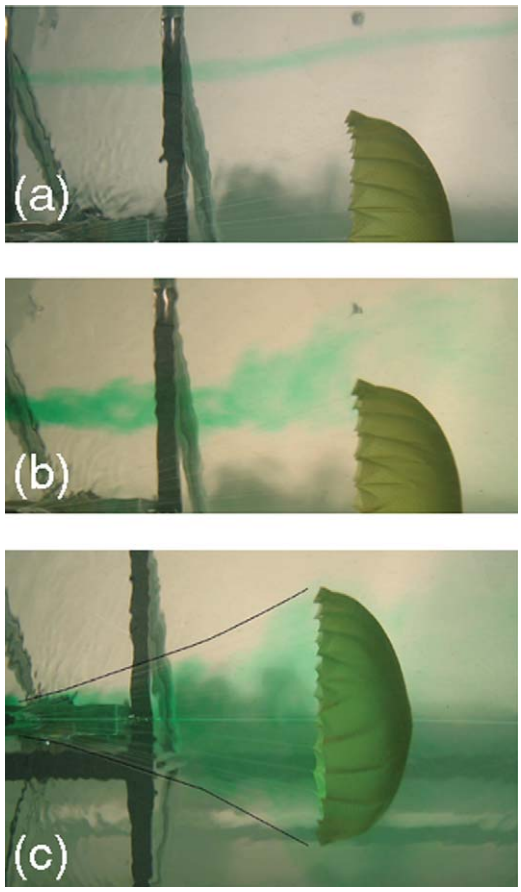

Fig. 4. Interaction of a line vortex with the 12-in canopy. Vortex is (a) outside the canopy; (b) on the lip of the canopy; (c) near the centerline. Dye released at the wing tip marked the vortex core.

coefficient was reasonably constant. The data for the two lowest Reynolds numbers had larger uncertainties, and these cases were not considered for the vortex interaction experiments.

The fluctuating component of drag is shown in Fig. 7 for $\mathrm{Re} > 3 \times 10^4$. As the Reynolds number increases, the root-mean-square (rms) of the fluctuating drag coefficient is reduced. At the highest Reynolds number of 9.1×10^4, the rms of C_D fluctuations is about 0.05. This value corresponds to 5% of the average drag for this case. Alternatively, large fluctuations of the drag, up to ~40%, are present at a Reynolds number of 3×10^4. The two cases with Reynolds number less than 3×10^4 had large rms values and were not considered further due to the large measurement uncertainties. Even for the case with the largest fluctuations in Fig. 7, the average drag coefficient has a standard error of less than 1% given the very large samples (20 000) collected for each case.

4.3. Effect of vortex interaction on the average drag

The variation of the time averaged drag coefficient with the spatial separation between the vortex and the canopy centerline, s/D_p, is presented in Fig. 8 for the three model canopies. For each freestream velocity, the relative vortex strength, $\Gamma/2\pi\sigma U$, and the vortex core size to canopy diameter ratio, σ/D_p, were constant. The vertical line in each plot indicates the location where the vortex center is exactly one forebody diameter from the canopy and forebody centerline. Data points to the left of the vertical lines are those that were significantly affected by the presence of the forebody whereas those to the right of the vertical lines were minimally affected by the forebody. As the vortex gets past the location indicated by the vertical lines, flow visualization revealed that the core disintegrates before reaching the canopy opening. The average drag coefficient for the 12-in canopy at Reynolds numbers of 6.1×10^4 and 9.1×10^4 is shown in Fig. 8(a). For both Reynolds numbers, the average drag decreases as the vortex core moves into the canopy

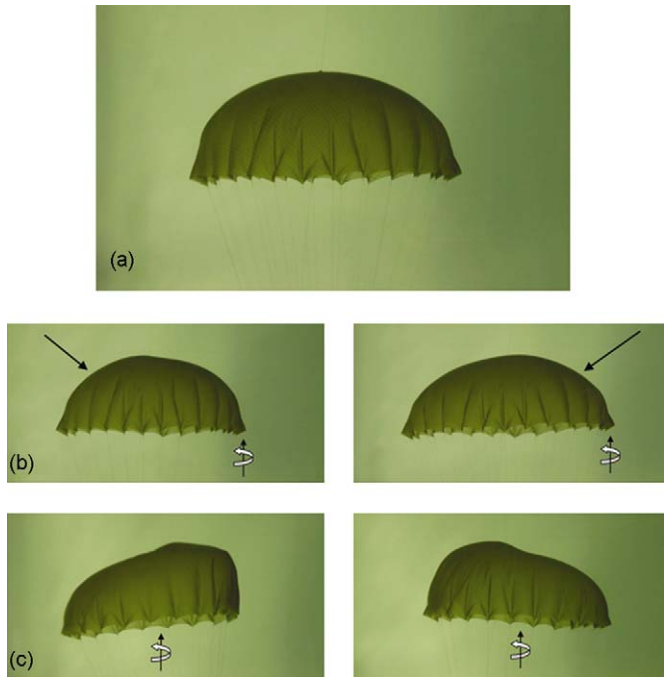

Fig. 5. Deformation of the 12-in model canopy as a result of the interaction with a vortex: (a) baseline, no vortex; (b) vortex at canopy lip; (c) vortex near the centerline. The curled arrows indicate the approximate location and sense of the vortex.

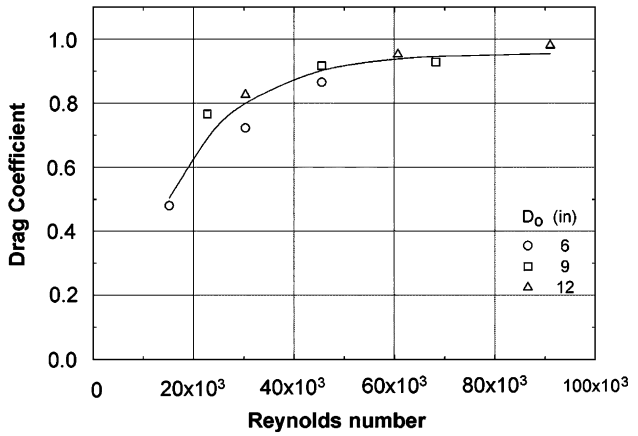

Fig. 6. Time-averaged drag coefficient of the canopy without vortex.

opening, $s/D_p < 0.5$. A minimum drag is reached when the vortex core is nominally at $s/D_p \approx 0.1$. This minimum value is approximately 12% less than the drag when the vortex is outside the canopy opening. As the vortex moves even closer to the canopy centerline and past the vertical line, the drag increases. Even when the vortex is outside of the canopy opening ($s/D_p > 0.5$), the presence of the vortex reduces the average drag by about 4%.

The two smaller canopy models exhibited a similar trend. As the vortex core moves toward the canopy centerline, drag reaches a minimum value which was 13% (9-in) to 19% (6-in) less than the value when the vortex is outside the canopy. For these smaller canopies, drag increases rapidly when the vortex core nears the forebody. Note that the baseline drag values are about 10% greater than the drag when the vortex is one diameter away from the canopy centerline. The data indicate that the presence of the vortex within the canopy opening reduces the mean drag for all cases studied. The minimum drag is observed when the vortex core is at 0.10–0.15 D_p away from the centerline. It is

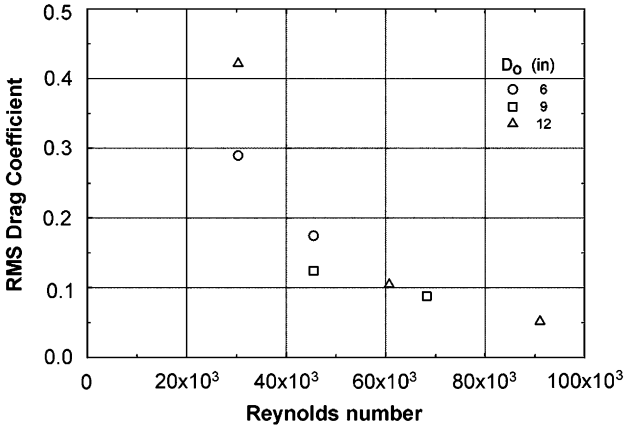

Fig. 7. Fluctuating component of the canopy drag without vortex.

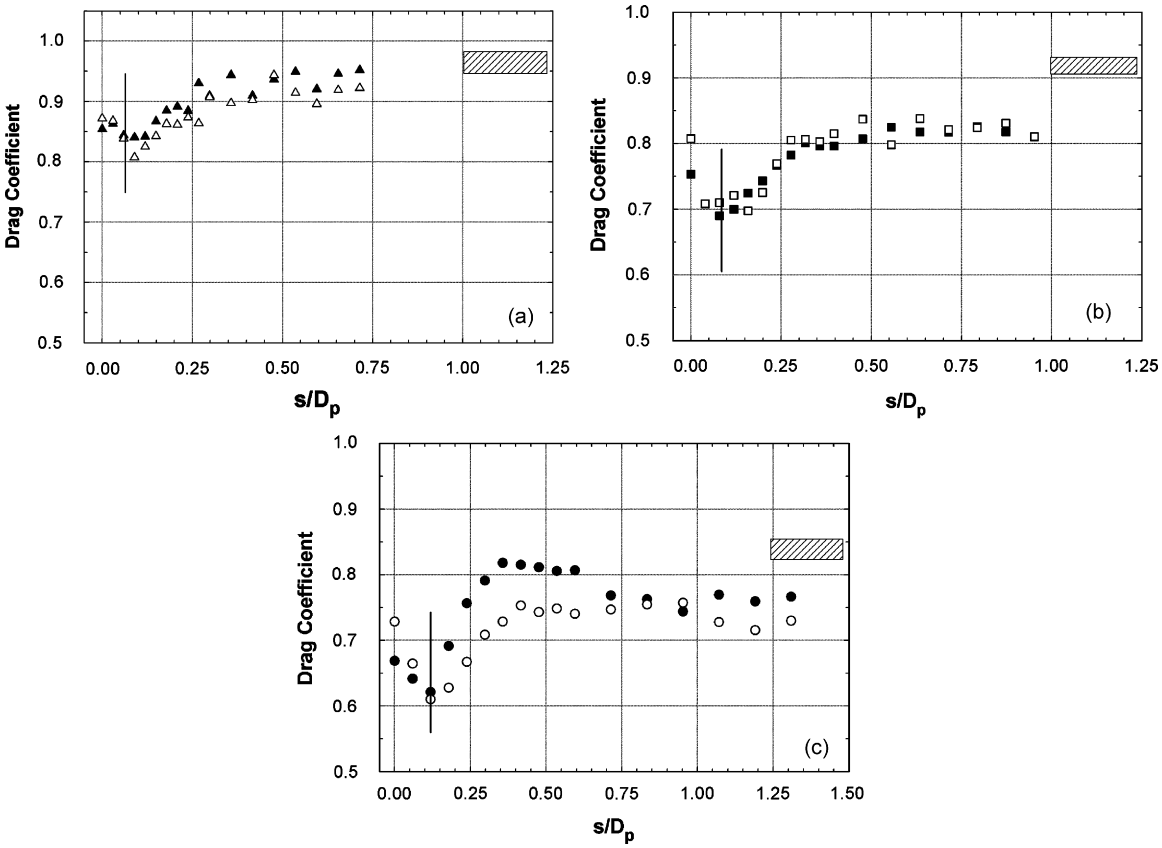

Fig. 8. Time-averaged drag coefficient as a function of the spatial separation between vortex axis and canopy centerline: (a) 12-in, (b) 9-in, (c) 6-in canopy. The shaded area is the range of the baseline data. The filled and open symbols refer to $U = 0.3$ and 0.2 m/s freestream velocities, respectively.

important to reiterate that the large number of samples taken at each point results in standard error values of less than 1% for the average drag despite the fairly large fluctuations. Thus, the observed decreases in the average drag are significant indeed. The data in Fig. 8 also indicate that the Reynolds number effects are much weaker for the two larger canopies than for the 6-in canopy model.

4.4. Fluctuating drag component

The rms of fluctuating drag for the three canopy models at freestream velocities of 0.2 and 0.3 m/s are shown in Fig. 9 The data for the 12-in canopy in Fig. 9(a) reveal that the fluctuating component of drag increases when the vortex is located at $s/D_p < 0.25$. As the vortex moves closer to the canopy centerline, the rms of drag coefficient experiences a peak which is about 80–100% greater than the values when the vortex is placed outside the canopy opening at the same Reynolds numbers. The larger drag fluctuations occur concurrently with the reduction in the average drag and are attributed to the unsteadiness associated with the vortex breakdown when the core is within the canopy opening. Once the vortex gets close to the centerline, the disintegration of the vortex core at the forebody partially relieves the increased drag fluctuations.

The relative increase in the drag coefficient fluctuation values for the 9-in canopy, shown in Fig. 9(b), at the higher Re is comparable to that of the 12-in canopy; however, at the lower Re the relative rise in $C'_{D\ \mathrm{rms}}$ is less than that for the 12-in canopy. The increase of $C'_{D\ \mathrm{rms}}$ starts when the vortex core reaches within $s/D_p < 0.25$. The maximum drag fluctuations are 15% and 40% larger than the values when the vortex is outside the canopy opening for the Reynolds numbers of 4.6×10^4 and 6.8×10^4, respectively. The data in Fig. 9(c) indicate that the 6-in canopy did not experience an appreciable change (<10%) in the fluctuating component of drag as the vortex core interacted with the canopy. This observation holds for both 3.0×10^4 and 4.6×10^4 Reynolds numbers. Interestingly, the $C'_{D\ \mathrm{rms}}$ plateau values for all the models when the vortex is outside the canopy opening is greater than the baseline values in Fig. 7. However, the 6-in canopy has much higher $C'_{D\ \mathrm{rms}}$ plateau values when compared to the baseline than the two larger canopy models.

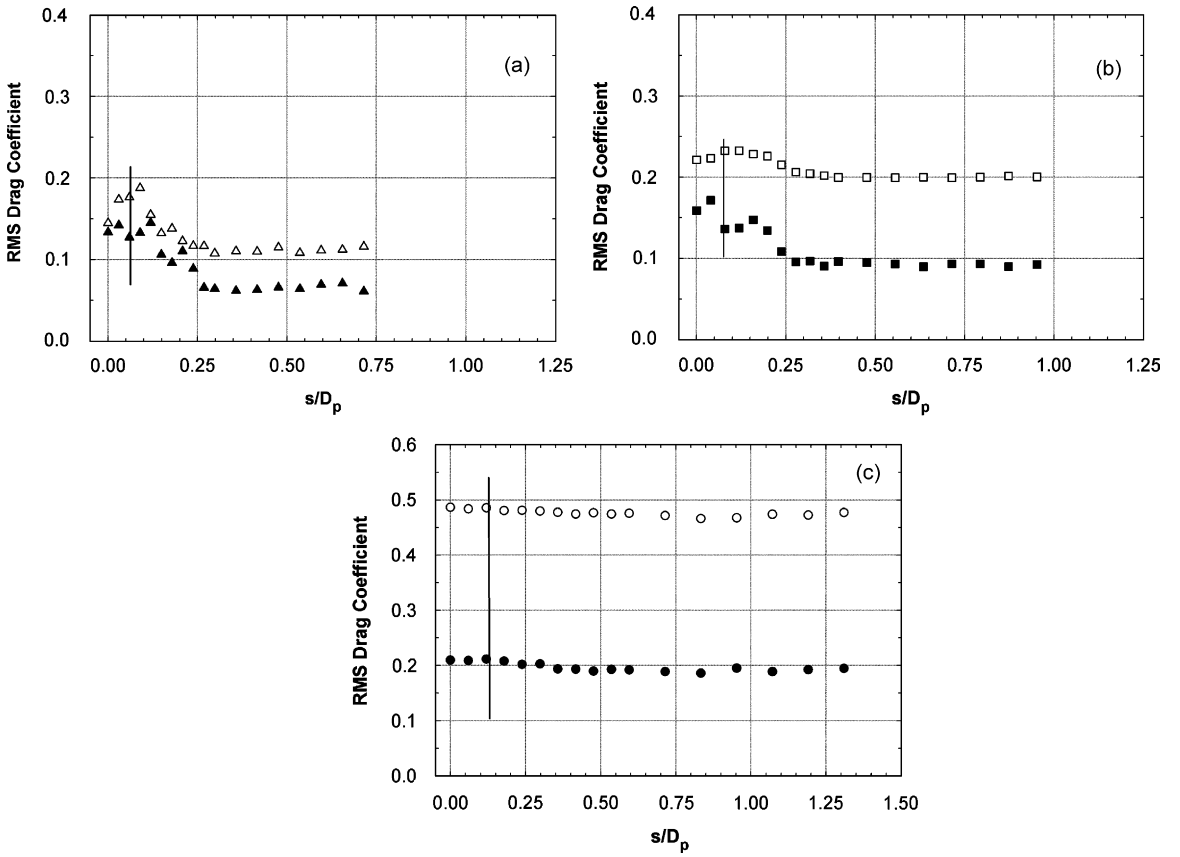

Fig. 9. Fluctuating component of drag as a function of the spatial separation between vortex axis and canopy centerline: (a) 12-in, (b) 9-in, (c) 6-in canopy. The filled and open symbols refer to $U = 0.3$ and 0.2 m/s freestream velocities, respectively.

4.5. Effect of vortex core size

To assess the effect of the relative vortex core size, the time averaged and fluctuating drag coefficients for cases with similar Reynolds numbers but different σ/D_p values are plotted in Figs. 10 and 11 The data for the 9- and 12-in models in Fig. 10(a) have Reynolds numbers $Re = 6.8 \times 10^4$ and 6.1×10^4, respectively. The corresponding relative core sizes are $\sigma/D_p = 0.10$ and 0.09 for the two data sets in Fig. 10(a). The data in Fig. 10(b) for the 6- and 9-in models have the same Reynolds number $Re = 4.6 \times 10^4$, but the relative core sizes are $\sigma/D_p = 0.15$ and 0.12. Both plots indicate a larger decrease in the time averaged drag and lower minimum values for the data with the larger σ/D_p values. The position where the minimum drag is generated is nearly independent of the vortex core size parameter. Same is also true for the position beyond which drag reduction initiates.

The fluctuating component of drag for the two larger canopies at similar Reynolds numbers is shown in Fig. 11 for the same parameters as in Fig. 10(a). The two data sets reveal that the peak values of $C'_{D\ \mathrm{rms}}$ are 70% and 85% greater than the plateau values for the 12- and 9-in models when the vortex core lies outside the canopy opening. The larger relative vortex core size of the 9-in canopy appears to have induced slightly greater drag fluctuations. For both sets, the vortex location where the rise in $C'_{D\ \mathrm{rms}}$ starts and the location of peak values are independent of the relative core size σ/D_p. Due to the small relative changes in the drag fluctuations of the 6-in model, the comparison with the 9-in model at the same Reynolds number was not carried out. Thus, increasing the relative core size, at least for the range examined in this study, has the effect of lowering the minimum time averaged drag values and increasing the maximum drag fluctuations by modest amounts.

5. Discussion

The observed vortex breakdown upstream of the canopy when the vortex trajectory falls within the canopy opening is due to the large pressure gradient experienced by the streamtubes approaching the canopy opening. Pressure rises

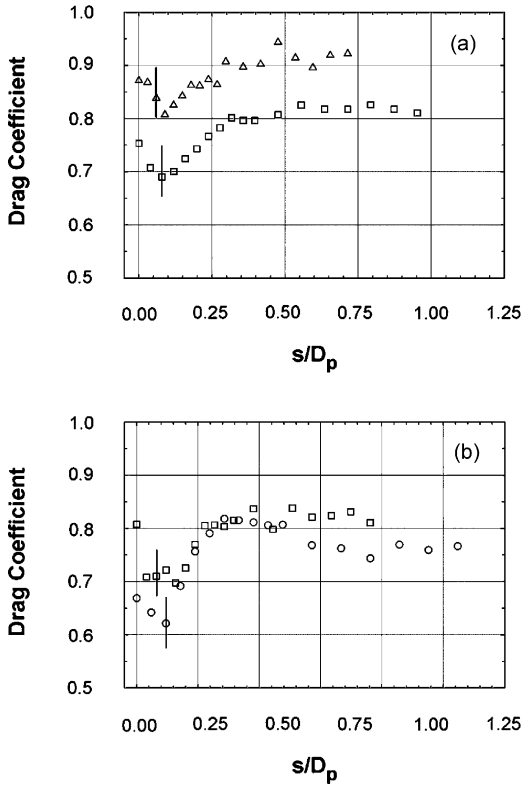

Fig. 10. Dependence of the time averaged drag coefficient on spatial separation between the vortex axis and the canopy centerline: (a) 12-in canopy (Δ) at $Re = 6.1 \times 10^4$, and 9-in canopy (□) at $Re = 6.8 \times 10^4$; (b) 9-in canopy (□) and 6-in canopy (○) at $Re = 4.6 \times 10^4$.

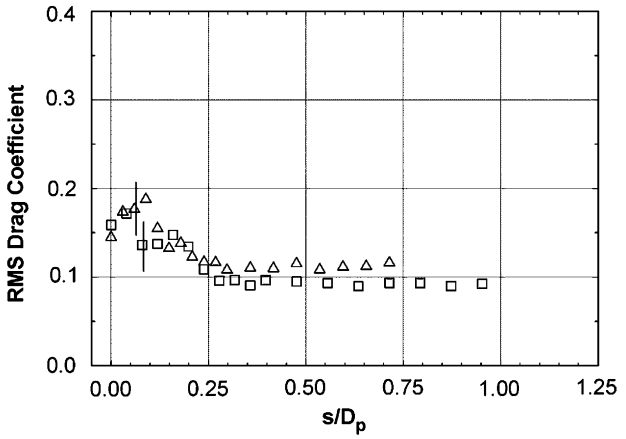

Fig. 11. Dependence of the fluctuating drag component on spatial separation between the vortex axis and the canopy centerline: 12-in canopy (Δ) at $Re = 6.1 \times 10^4$, and 9-in canopy (□) at $Re = 6.8 \times 10^4$.

rapidly from slightly above the freestream value at about one canopy projected diameter upstream of the opening to near the stagnation value within the canopy (Johari et al., 2001). This large adverse pressure gradient contributes to the observed helical-type vortex breakdown (Hall, 1972; Leibovich, 1978). Furthermore, in open flows such as in this experiment, vortex breakdown usually exhibits non-axisymmetric modes.

Even though the pressure in the core after vortex breakdown is greater than that in the initially tightly wound vortex (which has a pressure deficit comparable to the freestream dynamic pressure in the setup), it is still less than the stagnation pressure on the inner surface of the canopy. The pressure deficit in the vortex core results in the measured drag reductions in Fig. 8. When the vortex trajectory is near the canopy lip, the effects of low pressure vortex core on drag are minimal since the area on which the vortex acts is at an angle to the vortex core. As the vortex moves further inside, the canopy area affected by the vortex becomes nearly perpendicular to the vortex axis and the drag reduction increases. The effect of low pressure in the vortex core on the canopy drag is also corroborated by the observation that drag reduction is greater for the smaller canopy models. A larger fraction of the canopy surface is affected by the low pressure vortex core in the smaller models. Moreover, the data in Fig. 8 show that for all three canopy models the rapid drag reduction is initiated when the vortex core is at $\sim 0.3D_p$ away from the canopy axis. This further confirms the observed effect of the relative geometry between the vortex and canopy.

The minimum average drag is expected to occur when a low pressure vortex core interacts with a large cross-sectional area of the canopy. Ideally, this would take place when the vortex core is perpendicular to the canopy. However, the presence of the forebody prevents it. Then, the minimum is observed at the location where the forebody effects are minimal and the relative angle between the core and the canopy surface is not far from perpendicular. The location of the vortex breakdown also plays a role since it is expected that the pressure deficit in the vortex core decays in the downstream direction. In the current set-up, the location of vortex breakdown did not vary significantly, and hence, a notable effect from the vortex breakdown location is not expected in the data.

Although the vortex interaction results in a reduction in the time averaged drag of the canopy, the rms fluctuations of drag increase when the vortex is present within the canopy. The initiation of the rise in the drag fluctuations and the peak values occur at the same vortex positions where changes in the mean drag and minimum drag are observed, respectively. The unsteadiness associated with the vortex breakdown is responsible for the increased drag fluctuations. The largest increases in drag fluctuations are measured for the larger canopy models; on the other hand, the relative increase is minimal for the smallest model. As the smallest canopy model had large drag fluctuations even in the absence of the vortex, see Fig. 7, the presence of the vortex within the canopy adds little to the already large drag fluctuations. Since Reynolds number varies with the canopy scale, larger Reynolds number cases are affected to a greater extent by the vortex interaction. It is expected that full-scale parachute canopies to be much closer to the larger Reynolds number cases in the experiment. As the average drag is an integrated measure, the relative effect of Reynolds number on the average drag is substantially less.

It is also notable that time averaged drag when the vortex is outside the canopy is less than the baseline conditions. The reduction ranges from 4% for the largest canopy model to ~11% for the two smaller models. When the vortex core

is one half diameter outside the canopy edge, $s/D_p \approx 1$, the induced suction pressure is estimated to be only a few percent of the freestream dynamic pressure. Thus, direct pressure effects are unlikely to cause the observed drag reduction when the vortex is outside the canopy. It is thought that the swirling flow induced by the vortex changes the effective angle between the streamlines and the canopy axis, especially on the side closest to the vortex, and places a portion of the canopy at an angle of attack to the freestream. Hence, the reduced drag when the vortex is outside the canopy is claimed to be due to the tilting of the canopy with respect to the freestream.

The interaction of the vortex core with the forebody and its support structure causes the vortex to completely disintegrate into vorticity containing parcels when the trajectory of the vortex coincides with the forebody. The vortex core size σ is comparable to the diameter of the forebody and the support rod/shield. The vortical parcels subsequently interact with the canopy. Since the pressure deficit in the vortex core gets eliminated when the core disintegrates, the pressure reduction on the inside surface of the canopy is removed and the mean drag gets nearly restored. The disintegration of the vortex core near the canopy centerline also relieves the increased drag fluctuations brought on by the interaction of the coherent vortex with the canopy.

6. Conclusions

The interaction of a line vortex aligned with the axis of fully inflated model parachute canopies was studied experimentally for a range of Reynolds numbers and three laboratory scale canopy models. Flow visualization indicated that the core undergoes vortex breakdown when the core trajectory falls in the vicinity of the canopy lip or within the canopy opening. Vortex breakdown occurs about one to two canopy projected diameters upstream of the canopy opening. As the vortex core approaches the forebody, the vortex core completely disintegrates into large vortical parcels. The vortex breakdown and disintegration causes significant deformations on the canopy surface. The deformations appear to excite non-axisymmetric modes of the canopy. A reduction in the time averaged drag and an increase in the fluctuating drag is observed when the vortex core is within the canopy opening. For a given core size, canopies with smaller diameters experience a larger time-averaged drag reduction compared to larger canopies with similar Reynolds numbers. The change in the drag characteristics is observed at the same vortex core location for all canopies examined. The disintegration of the vortex core near the canopy centerline, due to the interaction with the forebody, eradicates the changes in drag brought about by the presence of the vortex core.

Acknowledgments

This project was sponsored by the US Army Research Office grant W911NF-05-1-0071 under technical direction of Dr T. Doligalski. The assistance of Drs K. J. Desabrais and E. Ghaem-Maghami during the experiments is greatly appreciated.

References

Blake, W., 1996. Prediction of paratroop/wake vortex encounters during formation airdrop. In: Proceedings of the AIAA Atmospheric Flight Mechanics Conference, AIAA Paper 96-3387.

Bodstein, G.C.R., George, A.R., Hui, C-Y., 1996. The three-dimensional interaction of a streamwise vortex with a large-chord lifting surface. Journal of Fluid Mechanics 322, 51–79.

Cockrell, D.J., 1987. The aerodynamics of parachutes. AGARDograph No. 295, AGARD-AG-295, AGARD. Neuilly sur Seine, France.

Desabrais, K.J., Johari, H., 1999. Reynolds number and scale effects on inflating parachute canopies. In: Proceedings of the 15th AIAA Aerodynamic Decelerator Systems Conference, AIAA paper 99-1736, pp. 258–268.

Gluck, M., Breuer, M., Durst, F., Halfmann, A., Rank, E., 2003. Computation of wind-induced vibrations of flexible shells and membranous structures. Journal of Fluids and Structures 17, 739–765.

Hall, M.G., 1972. Vortex breakdown. Annual Review of Fluid Mechanics 4, 195–218.

Heathcote, S., Wang, Z., Gursul, I., 2008. Effect of spanwise flexibility on flapping wing propulsion. Journal of Fluids and Structures 24, 183–199.

Heinrich, H.G., Hektner, T.R., 1971. Flexibility as a model parachute performance parameter. Journal of Aircraft 8, 704–709.

Johari, H., Stein, K., Tezduyar, T., 2001. Impulsively started flow about a rigid parachute canopy. Journal of Aircraft 38, 1102–1109.

Johari, H., Desabrais, K.J., 2003. Stiffness scaling for solid cloth parachutes. Journal of Aircraft 40, 631–638.

Johari, H., Desabrais, K.J., 2005. Vortex shedding in the near wake of a parachute canopy. Journal of Fluid Mechanics 536, 185–207.

Knacke, T.W., 1992. Parachute Recovery Systems Design Manual. Para Publishing, Santa Barbara, CA, USA (Chapter 5).
Lambert, C., Gursul, I., 2004. Characteristics of fin buffeting over delta wings. Journal of Fluids and Structures 19, 307–319.
Leibovich, S., 1978. The structure of vortex breakdown. Annual Review of Fluid Mechanics 10, 221–246.
Longatte, E., Verreman, V., Souli, M., 2009. Time marching for simulation of fluid–structure interaction problems. Journal of Fluids and Structures 25, 95–111.
Macha, J.M., Buffington, R.J., 1989. An experimental investigation of wall-interference effects for parachutes in closed wind tunnels. Sandia Report, SAND89-1485.
Maskell, E.C., 1965. A Theory of Blockage Effects on Bluff Bodies and Stalled Wings in a Closed Wind Tunnel. ARC R & M, Aeronautical Research Council, UK.
Peterson, C.W., Strickland, J.H., Higuchi, H., 1996. The fluid dynamics of parachute inflation. Annual Review of Fluid Mechanics 28, 361–387.
Rockwell, D., 1998. Vortex-body interactions. Annual Review of Fluid Mechanics 30, 199–229.
Rogers, L.C., Kididis, A.S., 1997. Parachute/vortex interaction study: Initial wind tunnel and drop testing. In: Proceedings of the 14th AIAA Aerodynamic Decelerator Systems Technology Conference, AIAA paper 97-1479, pp. 203–213.
Selig, M.S., Donovan, J.F., Fraser, D.B., 1989. In: Stokely, H.A. (Ed.), Airfoils at Low Speeds. Virginia Beach, VA, USA, pp. 260–261.
Strickland, J.H., Higuchi, H., 1996. Parachute aerodynamics: an assessment of prediction capability. Journal of Aircraft 33, 241–252.
Sun, M., Marshall, J.S., 2000. A flow visualization study of vortex interaction with the wake of a sphere. ASME Journal of Fluids Engineering 122, 560–568.
Wolfe, S., Lin, J.-C., Rockwell, D., 1995. Buffeting at the leading-edge of a flat plate due to a streamwise vortex: Flow structure and surface pressure loading. Journal of Fluids and Structures 9, 359–370.